Quantum-optical characterization of single-photon emitters created by MeV proton irradiation of HPHT diamond nanocrystals

Quantum-optical characterization of single-photon emitters created by MeV proton irradiation of HPHT diamond nanocrystals

E. Moreva[1], P. Traina[1], A. Tengattini[2,3], F. Picollo[2,3], A. Battiato[2,3], S. Ditalia Tchernij[2,3], I. P. Degiovanni[1], G. Brida[1], M. Genovese[1,3], P. Olivero[2,3], J. Forneris[3,2]*

(1) Istituto Nazionale di Ricerca Metrologica (INRiM), Torino, Italy
(2) Physics Department and "NIS" Inter-departmental Centre, University of Torino, Italy
(3) Istituto Nazionale di Fisica Nucleare (INFN) sez. Torino, Italy

**corresponding author: forneris@to.infn.it*

Abstract

Deterministic single-photon sources are a fundamental tool for several emerging applications in quantum sensing and quantum metrology. In these fields, the exploitation of individual quantum systems could significantly improve the current measuring capabilities and define a new generation of standard measure units. In addition, the availability of nanoscale-sized single-photon emitters is also of considerable interest, as it enables a further integration with external structures or biological samples.
In this work, we investigate the role of MeV proton irradiation in the production of single-photon emitters based on the nitrogen-vacancy complex (NV center) in nanodiamonds (NDs). Powders of nitrogen-containing type Ib diamond nanocrystals with a median size distribution of 80 nm were irradiated with 2 MeV protons at 5×10^{13} cm^{-2} fluence with the purpose of creating vacancies and thus promote the formation of NV centers upon a subsequent thermal annealing. Following a suitable chemical processing, the ND powders were characterized in their opto-physical properties by means of a single-photon-sensitive confocal photoluminescence microscopy setup equipped with a "Hanbury Brown & Twiss" interferometer, enabling the measurement of the second-order autocorrelation function characterizing the PL emission. A comparison with two reference batches of unirradiated NDs powder, which only underwent the chemical, and the chemical and thermal treatment, respectively, enabled to assess the role of ion implantation in the production of single-photon sources in type Ib diamond nanocrystals.

1. Introduction

Single-photon sources (SPSs) play a key-role in the development of emerging quantum technologies [1,2]. In particular, diamond is an appealing material for SPSs fabrication, as its large energy band gap can host a wide range of optically active centers with appealing emission properties [3-4]. The negatively charged nitrogen-vacancy complex (NV^-) is arguably the most widely studied color center in diamond, due to its unique photo-physical properties (quantum efficiency, spin-sensitive transitions, high spin coherence time, etc.) at room temperature [5-6]. Even if an ideal SPS (i.e. an "on-demand" and efficient emitter of indistiguishable single photons at an arbitrarily fast repetition rate) is far from being realized due to several technological constraints, a vast effort from the scientific community is currently dedicated to the improvement in the performance of real sources [7], as well as to their integration in photonic devices [8-10] and to the development of reliable fabrication processes [11-12]. In this paper we report on the fabrication by MeV ion irradiation and subsequent quantum-optical characterization of SPSs based on single NV centers embedded in individual nanodiamonds (NDs). The availability of nanoscale-sized SPS systems is especially appealing for biological research and imaging [13-15], as well as high-sensitivity electromagnetic field sensors [16-17] and quantum key distribution applications [18]. The irradiation protocol was implemented on a batch of NDs powder characterized by a small fraction of particles containing native NV centers. At the same time, the investigated NDs were characterized by a moderately high concentration of native substitutional N, being classified as "type Ib" according standard nomenclature in diamond science. The SPSs creation was therefore achieved upon the introduction of lattice vacancies through radiation damage and a subsequent annealing, with the purpose of promoting the formation of nitrogen-vacancy complexes [19-21]. The typical emission properties of NV-based SPSs in NDs is then presented and discussed. Finally, as the thermal annealing process in itself was reported to result in the formation of NV centers even in unirradiated samples [22], we also investigated the abundance of SPSs in a NDs powder batch which underwent only the thermal treatment.

2. Experimental

2.1 Samples fabrication. The material used in this work is a batch of synthetic NDs produced by ElementSix by disaggregation of High Pressure High Temperature (HPHT) synthetic diamond. The nominal size of individual NDs is comprised between 10 nm and 250 nm, with a median size of $d = (80 \pm 2)$ nm, as determined by X-Ray Diffraction (XRD) analysis of a powder sample (data not reported here). The NDs are classified as type Ib, their nominal substitutional N concentration being 100 ppm. Complementarily, the NDs are characterized by a low concentration of native vacancy defects, resulting in a low concentration of native NV centers. Therefore, the introduction of irradiation-induced vacancies and a subsequent thermal treatment were exploited for the formation of NV centers in NDs.

Firstly, ND powders were exposed to an acid bath (H_2SO_4:HNO_3 = 9:1 solution) for 72 hours at 100 °C before irradiation, with the purpose of removing possible surface organic contaminations and graphitic phases [23]. After filtering, the acid solution with the ND dispersion was neutralized in NH_3. The chemical reaction led to the formation of (NH_4)+NH_3^- salts, which were removed by diluting the samples with distilled water. The diluted solution was exposed to a sonic bath for 30 minutes, in order to obtain a homogeneous suspension. A centrifugation at 10,000 rpm for 15 min finally removed the remaining residuals of the chemical processing. The afore-mentioned chemical treatment was repeated three times for each NDs batch.

The processed NDs were deposited and pressed on a silicon substrate to form a ~10 µm film for the subsequent ion irradiation process. The irradiation was performed at the AN2000 accelerator of the INFN - National Laboratories of Legnaro (Italy), where several beamlines are available for the fabrication and characterization of materials [24-26]. The samples were irradiated with a 2 MeV proton broad beam over a 7×7 mm^2 area, with a 5 nA ion current.

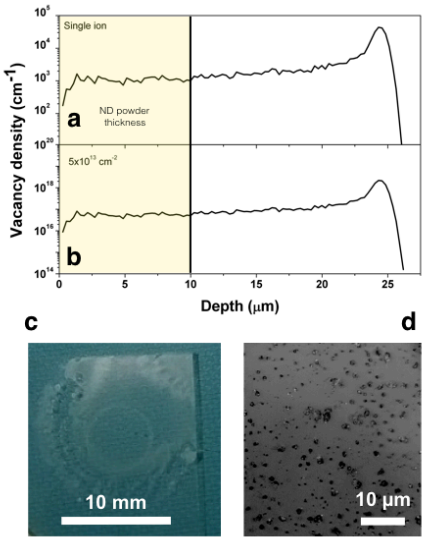

Figure 1: Vacancy densities (ρV) versus penetration depth in diamond, as evaluated by SRIM 2013 Monte Carlo code: **a)** linear density for a single implanted proton; **b)** volumetric density corresponding to a 5×10^{13} cm^{-2} fluence. The thickness of the ND layer is superimposed for clarity. **c)** Optical image of the silica cover-glass with dispersed nanodiamonds. **d)** optical micrograph of the dispersed NDs distribution.

In a statistical approach, the irradiation fluence was chosen to maximize the production of individual NV centers in each ND. The substitutional nitrogen concentration was assumed to be equal to $\rho_N = 1.77\times10^{19}$ cm^{-3} (corresponding to 100 ppm, according to the supplier specifications). The median volume of a ND with a 80 nm diameter (V_{ND} = 2.7×10^{-16} cm^3) was considered. The λ_v value was assumed to be constant within the whole depth of the deposited ND layer, as the penetration depth of protons in diamond is (24.3 ± 0.5) µm, and therefore the layer thickness does not overlap the Bragg's peak. The average volumetric vacancy density ρ_V across the irradiated volume (**Fig. 1b**) was then evaluated by multiplying the ion fluence F with a corresponding average linear vacancy density of $\lambda_v = 10^3$ vacancies cm^{-1} ion^{-1} (**Fig. 1a**) The latter value was estimated with the SRIM 2013.00 Monte Carlo code [27] in "Detailed damage calculation" mode, after having set the diamond displacement energy to 50 eV [28] and an average mass density of 3.52 g cm^{-3} for the diamond film. The fluence value was determined by the need of statistically introducing a single vacancy in each nanodiamond, i.e. $F = \lambda_v^{-1} \times V_{ND}^{-1} =. 5\times10^{12}$ cm^{-2}. However, a 10% NV centers creation yield needs to be taken into account [29], therefore the fluence value was rounded to $F = 5\times10^{13}$ cm^{-2}. After ion irradiation, the samples were annealed at 800 °C for 1h in a 800 mbar controlled N_2 atmosphere, to induce the formation of the NV centers. Subsequently, an additional cleaning step (30 min sonic bath in H_2SO_4, followed by a cleaning in "Piranha" solution) ensured the effective removal of organic residuals, metal oxides and carbonate deposits from the samples.

The ND powders were finally dispersed on a cover-slip silica glass substrate (Sample #1) for their optical characterization. The deposition was performed at $T > 340$ °C (.i.e. the sulfuric acid boiling point) to allow the liquid to evaporate, thus leaving a homogeneous ND dispersion over the substrates. An optical image of Sample #1 is displayed in **Fig. 1c**. A typical optical micrograph of the dispersed NDs with a 100× air objective is reported in **Fig. 1d**.
In order to assess the role of ion irradiation and of chemical processing, two additional samples were investigated. Sample #2 did not experience proton irradiation, but still underwent the same chemical and thermal treatment

performed on Sample #1 prior and after ion irradiation. Likewise, Sample #3 underwent the chemical processing only, i.e. without experiencing neither irradiation nor thermal annealing.

2.2 PL characterization. The photoluminescence characterization of samples was performed with a single-photon-sensitive confocal PL microscopy setup with a custom acquisition software [30]. The excitation radiation was provided by a solid state Nd:YAG pulsed laser at 532 nm by PicoQuant (10 MHz repetition rate, <100 ps pulse width). The main optical elements adopted in the confocal microscope setup included a long-pass dichroic mirror (edge wavelength: 567 nm), a 100× oil-immersion objective (1.3 N.A.) and a 650 nm long-pass filter. The detection system consisted of two independent Perkin-Elmer SPCM-AQR-15 single-photon avalanche detectors (SPADs) connected to the confocal microscope through a fiber-coupled 50:50 beam-splitter to form a Hanbury Brown & Twiss (HBT) interferometer, feeding a IDQ800 multi-channel time tagger. The latter was adopted both as a counter for PL mapping and as the time-to-digital converter of the HBT interferometer. The samples were mounted on a three-axes closed-loop piezo-electric stage with <5 nm resolution. PL spectra were acquired with a Princeton Instrument Acton SP-2150 monochromator, with a 1200 grooves mm^{-1} grating and a spectral resolution of ~2 nm.

Results and discussion

3.1 Single-photon emission. A typical 80×80 μm^2 PL intensity map acquired from a ND dispersion of Sample #1 is reported in **Fig. 2**. All the different probed regions exhibited similar features, consisting of several isolated luminescent spots (~30 kcps emission intensity) with sub-micrometer size surrounded by a low background emission from the silica substrate. By means of HBT interferometry, the spots could be identified as individual NDs containing single color centers, while several larger and significantly brighter (up to ~Mcps intensity) regions revealed the presence of NDs clusters due to their aggregation during the deposition process. The distribution in size and density of individual NDs and ND clusters was observed to be homogeneous on all the samples investigated in this work.

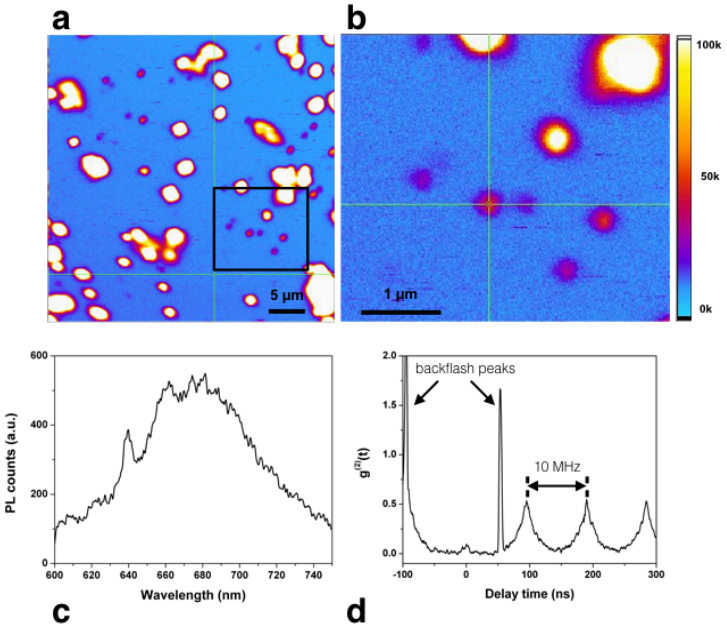

Figure 2: Confocal PL microscopy characterization of single-photon emitting NDs. **a)** Typical 2-dimensional 80×80 μm^2 PL map acquired from Sample #1. **b)** Magnification of the region highlighted by the black square in Fig. 2a. **c)** PL spectrum of the single-photon emitting ND with the typical features of the NV^- emission. **d)** Typical background-subtracted second-order autocorrelation chronogram $g^2(t)$ of the coincidence events at the two outputs of the Hanbury Brown & Twiss interferometer, acquired from the single-photon emitting ND highlighted by the crossbar in Fig. 2b. Measurements were acquired under 10 MHz pulsed 532 nm laser excitation. The spacing between the peaks of the $g^2(t)$ function correspond to the period of the pulsed excitation.

The magnification of the confocal PL map in **Fig. 2b** (taken from the region highlighted by the black square in **Fig. 2a**) exhibits the presence of several individual NDs, which displayed a stable photoemission over time. The analysis of the PL emission from a typical ND SPS is shown for the spot highlighted by the crossbar in **Fig. 2b**. Its PL spectrum (**Fig. 2c**) revealed the typical emission of the negative charge (NV^-) state of the nitrogen-vacancy complex, with a pronounced zero-phonon line at 638 nm and its phonon replica at higher wavelengths [5].
Second-order autocorrelation function measurements (**Fig. 2d**) were performed to determine the non-classical features of the PL emission.. The spacing between the peaks observed in the coincidences chronogram corresponds to the period of the pulsed excitation. The observation of a smaller peak at zero delay time indicates the presence of non-classical emission, i.e. the impossibility for the point source under analysis of emitting two photons at the same time [31]. The two narrow peaks at t ~ 55 ns and t ~ -95 ns are associated with the backflash photons, emitted during the charge carriers avalanche of the detecting SPADs pair [32,33]. In order to quantify the non-classicality of the emitter, the data

were normalized according to the procedure described in [34]. The $g^{(2)}(t=0) = 0.10$ value was finally determined, as the ratio between the area underlying the zero-delay peak ($\Delta t = 0$) and the corresponding value associated with the next pulse repetition (i.e. the one centered at Δt =100 ns delay). The emission lifetime of the SPS was directly estimated by a fit of the single exponential decays in correspondence of the $g^{(2)}(t)$ coincidence peaks at $t \neq 0$, the pulse width being shorter than the expected lifetime.

3.2 *Single-photon emission properties.* The distributions of the $g^{(2)}(0)$ and emission lifetime values measured on a sample of 46 single-photon-emitting NV centers embedded in individual NDs in Sample #1 are displayed in **Figs. 3a** and **3b**, respectively. Second-order autocorrelation values exhibited a wide variability in the 0.05-0.5 range, typically depending on the local enviroment such as background luminescence, scattered light from surrounding nanocrystals and substrate surface inhomogeneities. Nevertheless, $g^{(2)}(0) < 0.15$ values such as the one reported in **Fig. 2d**, were not uncommon. Remarkably, NV centers with $g^{(2)}(0)$ values as low as <0.04 were measured on Sample #1.

Similarly, the emission lifetime distribution (**Fig. 3b**) also exhibits a wide variability in the 13-31 ns range, spanning from the typical values of NV centers in bulk diamond (~12 ns, [35]) to those of ND-embedded emitters (i.e. ~19-25 ns [35-36]). This latter effect was attributed in previous works to the Purcell effect, i.e. to the increase in the refractive index surrounding the emitter [37]. The dispersion in the emission lifetime may be attributed to the position of the NV center relative to the ND/silica interface, as well as to the randomness of the dipole orientation [37].

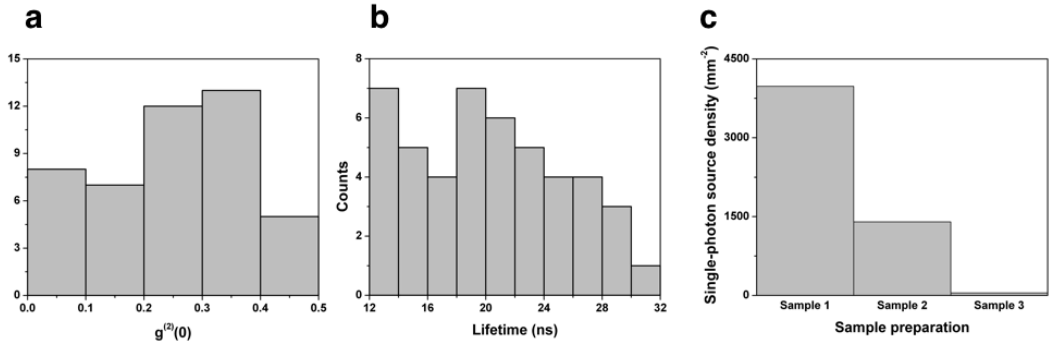

Figure 3: a) Distribution of $g(2)(t=0)$ over a population of 46 single-photon emitting NV centers embedded in individual NDs from Sample #1. **b)** Distribution of the emission lifetime of the same set of NV centers. **c)** Estimated density of single-photon sources per square millimeter in Sample #1 (irradiated with protons at fluence), Sample #2 (chemically and thermally processed) and Sample #3 (as deposited).

3.3 The role of ion implantation. A systematic PL mapping of Samples #1-3 enabled to assess the role of the ion irradiation and of the chemical and thermal treatments on the formation of SPS based on NV centers in NDs. In **Fig. 3c** the density of SPSs per unit area is reported, under the assumption of a homogeneous ND dispersion in all the samples under investigation. The control Sample #3, which was chemically processed but neither irradiated nor annealed, exhibited a negligible density of single-photon emitters. Conversely, the density of single-photon-emitting NDs in Sample #1 was estimated as $\sim 4.0 \times 10^3$ mm^{-2}, i.e. significantly higher than that ($\sim 1.5 \times 10^3$ mm^{-2}) of unirradiated NDs which underwent both chemical and thermal processing (Sample #2). On the other hand, it is worth noting that the thermal treatment alone resulted in the formation of a non-negligible amount of NV centers, which is however boosted by the vacancy introduction provided by the ion irradiation process.

Conclusions

We reported on the fabrication of single-photon sources based on NV centers embedded in nanodiamond crystals. Following a preliminary chemical processing, Ib-type nanodiamond powders with ∅~80 nm size were irradiated with 2 MeV protons to introduce an optimal vacancy density for the statistical formation of individual optical centers in each ND upon thermal annealing. The PL confocal microscopy analysis of NDs dispersed on silica substrates allowed to assess the emission lifetime and the single-photon emission features of the NDs. This approach enabled the deposition of a high density (>4.0×10^3 mm^{-2}) of single-photon sources. The non-classicality of the single-photon emitters was evaluated through the measurement of the $g^{(2)}(0)$ value of the second-order auto-correlation function, which displayed a significant variability in the 0.05-0.50 range. Such a variability was ascribed to local features of the substrate (background luminescence, surface inhomogeneities) or to scattered light from surrounding ND clusters. The emission lifetime also displayed a significant variability, ranging from values close to those of NV centers in bulk crystal (13 ns) up to 31 ns, i.e. closer to the characteristic emission lifetime in NDs (25 ns). A comparison with two reference ND samples, which respectively underwent only chemical processing, or a chemical processing and thermal annealing, enabled to assess that the ion irradiation provides a significant boost to the formation of single-photon sources in nanodiamonds with respect to the thermal processing. Nonetheless, the latter process was observed to provide a non-

negligible increment in the SPS concentration. The ease of production and the availability of large amount of cost-effective single-photon sources embedded in nanoscale-sized objects provides an appealing perspective for scientific and technological applications. Indeed, the unique sensing properties of the NV center, combined with the dimensions of individual nanodiamonds offers in perspective a tool for accurate field sensing and imaging at the nanoscale. The exploitation of "pick-and-place" approaches for addressing and integrating individual SPSs in photonic structures envisages promising applications in quantum optics and photonics domains [38,39]. Furthermore, we envisage the future employment of luminescent NDs in biomedical research, due to their non-toxicity and bio-compatibility, both as fluorescent markers [40,41] and sensing probes [42].

Acknowledgements

This research was supported under the following schemes: "DIESIS" project funded by the Italian National Institute of Nuclear Physics (INFN) - CSN5 within the "Young research grant" scheme; EMPIR Pro ject. No. 14IND05-MIQC2; Coordinated Research Project "F11020" of the International Atomic Energy Agency (IAEA); Project Q-SecGroundSpace. MeV H implantations were performed within the "Dia.Fab." experiment at the INFN-LNL laboratories.

References

[1] M. D. Eisaman et al., Rev. Sci. Instr. 82, 071101 (2011). doi: 10.1063/1.3610677.
[2] C. J. Chunnilall et al. Opt. Eng. 53(8) (2014) 081910. doi: 10.1117/1.OE.53.8.081910
[3] J.O. Orwa et al., Journal of Luminescence 130 (2010) 1646. doi: 10.1016/j.jlumin.2009.12.028.
[4] I. Aharonovich et al., Nature photonics 5 (2011) 397. doi: 10.1038/nphoton.2011.54
[5] M.W. Doherty et al., Physics Reports 528 (2013) 1. doi: 10.1016/j.physrep.2013.02.001
[6] R. Schirhagl et al., Annual Review of Physical Chemistry 65 (2014) 83. doi: 10.1146/annurev-physchem-040513-103659.
[7] B. Rodiek et al., Optica 4 (2017) 71. doi: 10.1364/OPTICA.4.000071
[8] T. Schröder et al., Journal of the Optical Society of America B 33 (206) B65. doi: 10.1364/JOSAB.33.000B65.
[9] J. Benedikter et al., Phys. Rev. Applied 7 (2017) 024031. doi: 10.1103/PhysRevApplied.7.024031.
[10] E. Ampem-Lassen et al., Optics Express 17 (2009) 11287. doi: 10.1364/OE.17.011287
[11] J. R. Rabeau, Nano Letters 7 (2007) 3433. doi: 10.1021/nl0719271.
[12] S. Pezzagna et al., New J. Phys. 13 (2011) 035024. doi: 10.1088/1367-2630/13/3/035024.
[13] Y. Chang et al., Nat. Nanotechnol. 3 (2008) 284. doi: 10.1038/nnano.2008.99.
[14] A. Hartl et al., Nat. Mater. 3 (2004) 736. doi: 10.1038/nmat1204.
[15] L. P. McGuinness et al.,Nat. Nanotech. 6 (2011) 358. doi: 10.1038/NNANO.2011.64.
[16] L. Rondin et al., Nature Communications 4 (2013) 2279. doi: 10.1038/ncomms3279.
[17] Y.-K. Tzeng et al., Nano Lett. 15 *(*2015) 3945. doi: 10.1021/acs.nanolett.5b00836.
[18] E. Wu et al., Opt. Express 14 (2006) 1296. doi: 10.1364/OE.14.001296.
[19] B. Naydenov et al., Appl. Phys. Lett., 96 (2010) 49. doi: 10.1063/1.3409221
[20] J. Botsoa et al., Phys. Rev. B 84 (2011) 125209. 10.1103/PhysRevB.84.125209.
[21] J.-P. Boudou et al., Nanotechnology 20 (2009) 235602. doi: 10.1088/0957-4484/20/23/235602.
[22] X. Song et al.,Appl. Phys. Lett. 102 (2013) 133109. doi: 10.1063/1.4823548.
[23] T. Gaebel et al., Diam. Relat. Mater. 21 (2012) 28. doi:10.1016/j.diamond.2011.09.002.
[24] A. Re et al. Nucl. Instr. Meth. B 348 (2015) 278. doi: 10.1016/j.nimb.2014.11.060.
[24] J. Forneris et al,. EPL 108 (2014) 18001. doi: 10.1209/0295-5075/108/18001.
[26] A. Quaranta et al., Spectrochimica Acta A 121 (2014) 1. doi: 10.1016/j.saa.2013.10.038.
[27] F. Ziegler, M.D. Ziegler, J.O. Biersack, *SRIM—the stopping and range of ions in matter*, Nuclear Instruments and Methods in Physics Research B 268 (2010) 1818. doi: 10.1016/j.nimb.2010. 02.091.
[28] D. Saada et al., Int. J. Mod. Phys. C 09 (1998) 61. doi. 10.1142/S0129183198000066.
[29] S. Pezzagna et al., New J. Phys. 12 (2010) 065017. doi: 10.1088/1367-2630/12/6/065017.
[30] J. Forneris et al., Sci. Rep. 5 (2015) 15901. doi: 10.1038/srep15901.
[30] D. Gatto Monticone et al., New J. Phys. 16 (2014) 053005. doi: 10.1088/1367-2630/16/5/053005
[32] A. Meda et al., Light 6 (2017) 6, e16261. doi:10.1038/lsa.2016.261.
[33] C. Kurtsiefer et al., J. Modern Opt. 48 (2001) 2039. doi: 10.1080/09500340108240905.
[34] R. Brouri et al., Opt. Lett. 25 (2000) 1294. doi: 10.1364/OL.25.001294.
[35] J. Storteboom et al., Optics Express 23 (2015) 11327. doi: 10.1364/OE.23.011327.
[36] M. Berthel et al., Phys. Rev. V B 91 (2015) 035308. doi: 10.1103/PhysRevB.91.035308.
[37] A. Beveratos et al., Phys. Rev. A 64 (2001) 061802. 10.1103/PhysRevA.64.061802.
[38] T. Schröder et al., Nano Lett. 11 (2011) 198. doi: 10.1021/nl103434r
[39] J.-P. Tetienne et al., Science 344 (2014) 1366. doi: 10.1126/science.1250113.
[40] K. Solarska-Sciuk et al., Chem.-Biol. Inter., 219 (2014) 90. doi: 10.1016/j.cbi.2014.05.013.
[41] G. Balasubramanian et al., Chem. Biol. , 20 (2014) 69. doi:10.1016/j.cbpa.2014.04.014
[42] T.M. Babinec et al., Nature Nanot. 5, 195 (2010). doi: 10.1038/NNANO.2010.6.